THE UNIVERSITY *of* EDINBURGH
School of Physics
and Astronomy

An Analysis of the Turbulence Spectrum at Varying Magnetic Prandtl Number

MPhys Project Report

Clara Despard

March 27, 2017

Abstract

An investigation of the magnetohydrodynamic turbulence has been conducted using direct numerical simulation, focusing on the Prandtl number dependence of the energy and dissipation spectra. A power law dependence of the dissipation ratio on the Prandtl number was found to be $\frac{\epsilon_u}{\epsilon_b} = 0.6Pr_m^{0.55}$ for decaying simulations. No power law dependence could be found from the results of the stationary simulations and reasons for this are discussed.

Supervisor: Professor A. Berera

Personal statement

I started my project by reading *Hydrodynamic Turbulence* by David McComb[1], and *Magnetohydrodynamic Turbulence* by Dieter Biskamp[2], to enhance my knowledge of this entirely new subject matter. I also installed the code by Yoffe et al.[3] on my laptop and read the accompanying documentation. By mid October I was running small ($N = 32$) simulations on my laptop. I used these to learn how to use the post processing scripts.

Unfortunately, due to delays with the Information Services, I did not get an account on `eddie` until late October. As a result, the decaying simulations for $N > 128$ were run by Mairi McKay as she showed me how to use write input files and submit job scripts.

As I began to analyse the decaying data, I worked with Mairi MacKay to decide on what forced/stationary simulations to run. Running these simulations took a while, as often errors with the input were not easy to spot until the data was post processed, and the simulation had to be run again. Access to `archer` was requested but not secured until the end of November, by which time most of the stationary data had been obtained from `eddie`.

In January, time was spent preparing the practise presentation and writing up the literature review. In addition I began to analyse the results of the stationary simulations. I learnt to use bash script so that I could understand the post processing scripts I had been given and write some of my own for finding the dissipation peaks and generating gnuplot scripts.

February was spent learning to use gnuplot, LaTeX, and paraview, the visualisation software used to generate images from the data. During this time I analysed my results alongside results in other recent studies, including Sahoo et al.[4] and Brandenburg et al.[5]. Additional simulations were run on `archer` to extend the decaying data to $Pr_m < 1$, and to create visualisations of the forced turbulence.

I discussed my results with Mairi and Prof. Arjun Berera and hypothesised as to why they might differ from the literature, but there was not time to run further simulations. Time since then has been spent generating graphs of the data and writing the report

Contents

1 Introduction

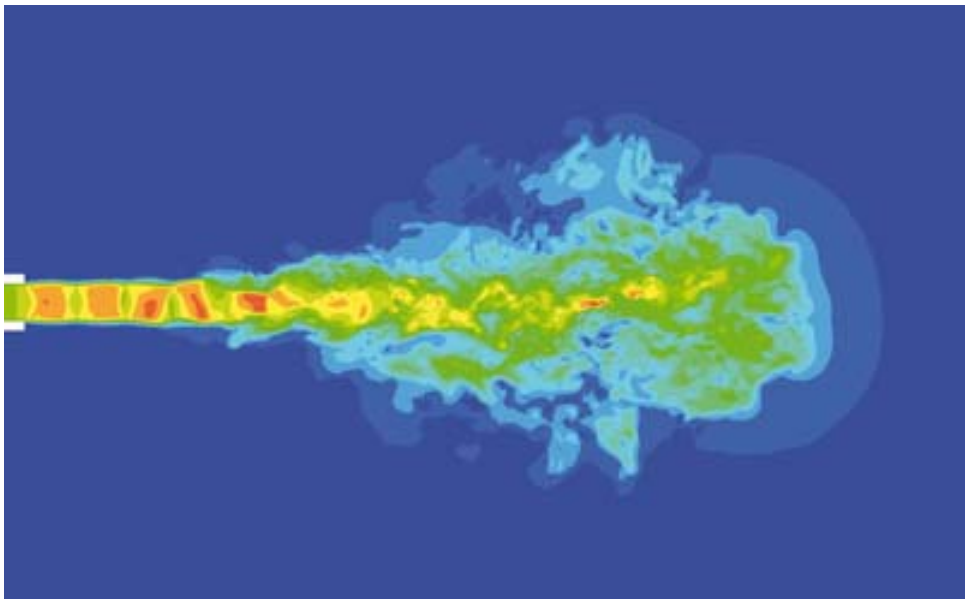

Figure 1. An example of turbulent flow in a pipe simulated on 2 million grid cells in 2 dimensions[6].

Turbulence is a phenomenon that has fascinated physicists and mathematicians alike for centuries, and finding solutions to the equations that govern fluid dynamics is still one of the biggest unsolved problems of our time; it is one of the seven Millennium Prize Problems in mathematics. However, even without the proof of the existence of a smooth unique solution, there is much to be learnt from computer simulations of fluid turbulence[1]. Unlike laminar flow, where the movement of fluid can be easily modelled as a continuum, turbulent flow is more challenging due to its chaotic nature. The transition from laminar to chaotic, turbulent flow can be seen in figure 1.

Magnetohydrodynamics (MHD) describes the flow of a fluid which conducts an electric charge. The movement of charge creates a magnetic field which in turn affects the dynamics of the fluid, thus further complicating the dynamics of the system. The transition to turbulence is governed by the Reynolds number (see section 2.1, equation 2.3), which can be viewed as a measure of how turbulent a system is. Magnetic fluids have both a kinetic and magnetic Reynolds number and the ratio of these two Reynolds numbers is known as the magnetic Prandtl number[2]. It is a measure of how turbulent the magnetic field is compared to the kinetic field.

Magnetic Prandtl numbers of physical substances vary hugely, from 10^{-6} (much more turbulent in the kinetic field than in the magnetic field) in the Earth's core, to 10^{12} (much more turbulent in the magnetic field) in the interstellar medium[7]. Simulating these situations with the degree of accuracy used in this project is not possible with the computational power at our disposal, as numerical simulations cannot be fully resolved at such extreme

Prandtl numbers[1]. This project will concentrate on Prandtl numbers between 0.1 and 10, and investigate whether any trends can be seen, and what can be extrapolated from that.

This project looks at non-helical decaying and stationary simulations of MHD. We aim to study the effects of varying the Prandtl number by looking at the energy spectra generated, and the rates of energy dissipation in both the magnetic and kinetic fields. Previous studies have looked at power laws relating the Prandtl number to the kinetic to magnetic dissipation ratio[5, 8, 4], which we attempt to verify and understand better, in addition to examining the energy and dissipation spectra, and the ratio of total energies.

Report Structure

To fully study the dynamics of MHD, the movement of non conducting fluids must first be understood, discussed in section 2. The MHD equations are then be introduced, and our analysis of turbulence extended to include MHD in section 3. The methods used to simulate the turbulence are explained in section 4, followed by a detailed analysis of results and some discussion and comparisons of the data. A glossary of important terms is provided at the end of this report (appendix A).

2 Dynamics and Turbulence in non-conducting fluids

2.1 Introduction to Fluid Dynamics

When modeling fluid flow on a macroscopic scale, the fluid is approximated as a continuum, rather than tracking the path of each individual particle. Fluid motion in continuum is governed by the **Navier-Stokes Equation**:

$$\frac{\partial \mathbf{u}}{\partial t} + (\mathbf{u} \cdot \boldsymbol{\nabla})\mathbf{u} = -\frac{1}{\rho}\boldsymbol{\nabla} P + \nu \nabla^2 \mathbf{u} + \mathbf{F_u} \tag{2.1}$$

which depends on the velocity field $\mathbf{u}$, density ρ, pressure P and viscosity ν[1]. $\mathbf{F_u}$ is an external force (e.g. gravity) acting on the fluid. The viscosity is an important quantity to consider when studying turbulence. It is an intrinsic property of the fluid that measures its resistance to deformation under an applied force[1]. Informally, it measures the 'thickness' or 'gloopiness' of the fluid. As is the case for all continuum mechanics, the curl of the velocity field measures the rotation of the fluid locally, and is referred to as the vorticity; $\boldsymbol{\omega} = \boldsymbol{\nabla} \times \mathbf{u}$[1].

To derive the Navier-Stokes equation, the fluid is assumed to be incompressible[1],

$$\boldsymbol{\nabla} \cdot \mathbf{u} = 0. \tag{2.2}$$

[1]Resolution of simulations is discussed fully in section 4.1

The $(\mathbf{u} \cdot \boldsymbol{\nabla})\mathbf{u}$ term in the Navier-Stokes equation is non-linear, and is what makes the solving the equation challenging. At relatively high velocities and low viscosities this term dominates the behaviour of the fluid. At relatively low velocities and high viscosities the $\nu\nabla^2\mathbf{u}$ term dominates, which describes energy dissipation through viscous forces into heat. Different behaviours arise depending on the dominant term in the equation. To understand this phenomenon clearly, a dimensionless parameter, the Reynolds number, is defined as

$$Re = \frac{UL}{\nu} \tag{2.3}$$

where U and L are, respectively, the characteristic velocity and characteristic length scale of the motion of the fluid, and ν is the viscosity as defined before[1].

The Reynolds number acts as a bifurcation parameter; a small change in this control parameter can qualitatively change the dynamics of the system as a whole[9]. When the Reynolds Number goes above a critical value, the flow changes from laminar to turbulent. In the neighbourhood of this critical value there exist flows that are topologically distinct, so that once this value is exceeded an entirely different behaviour is observed. For pipe flow, the Reynolds number must be above $Re_{\text{crit}} \simeq 2000$ to see turbulent behaviour[1]. However, for MHD, this value can be much lower, and for homogeneous isotropic MHD, turbulent behaviour can be seen at Reynolds numbers much lower than this, $Re_{\text{crit}} \simeq 100$.

2.2 Turbulence as a Statistical Problem

Although the Navier-Stokes equation completely describes the motion of the fluid, a unique smooth solution has not been found to describe a turbulent system. However, the system can be interpreted as stochastic, and analysed statistically. This involves taking averages over the probability density function, which will be denoted by angle brackets $\langle\ \rangle$.

To do so, the velocity is broken into $\mathbf{U} = \bar{\mathbf{U}} + \mathbf{u}$, where $\bar{\mathbf{U}}$ is the mean value of $\mathbf{U}$ and $\mathbf{u}$ are fluctuations on the mean, so $\langle \mathbf{u} \rangle = 0$. Substituting this into the Navier-Stokes equations gives the Reynolds equation (using index notation and the Einstein summation convention):

$$\frac{\partial \bar{U}_i}{\partial t} + (\bar{U}_j \partial_j)\bar{U}_i = -\frac{1}{\rho}\partial_i \bar{P} + \nu \partial^2 \bar{U}_i - \partial_j \langle u_i u_j \rangle + F_i \tag{2.4}$$

where terms are as defined for the Navier-Stokes equation, F_i is an external force, and $\langle u_i u_j \rangle$ is an apparent stress tensor, called the *Reynolds stress tensor*[1].

Symmetries are then introduced to the system before any further analysis of these equations can be done. The simplest way of doing this is to make the system spatially and rotationally invariant. Homogeneity refers to the invariance of a system under translations in space, and isotropy refers to the invariance of the system under rotations in space. The concept of **Homogeneous Isotropic Turbulence** (HIT) is purely theoretical, as it ignores all boundary conditions, but allows us to gain a phenomenological understanding of turbulence, as well as providing an approximate simulation of turbulence away from any effects of boundary conditions[1]. HIT can be generated in the lab using a wind tunnel, by a coordinate transform into a frame which moves with the flow. Under these conditions, $\bar{U}$ must be zero, and we need only look at the fluctuating part of the Reynolds equations.

2.3 Correlation Tensors

Correlation measures the effects of nearby velocities on the velocity at a certain point in space. If two points are sufficiently far away that the motion at one point has no effect on the motion at the other, these two velocities are said to be uncorrelated. The correlation between two velocities in space and time is given by a tensor, called the correlation tensor. Since the focus of this report is on homogeneous and isotropic turbulence, the correlation function must not depend on the individual positions, only on the distance between them. The correlation tensor can therefore be defined as[1]

$$C_{ij}(\mathbf{r}, t, t') = \langle u_i(\mathbf{x}, t) u_j(\mathbf{x} + \mathbf{r}, t') \rangle. \tag{2.5}$$

We can also define equal time correlation functions by setting $t = t'$ and dropping the time dependence from the correlation function, so it becomes $C_{ij}(\mathbf{r})$. To remove the directional dependence of $C_{ij}(\mathbf{r})$, and preserve isotropy, the parallel and perpendicular correlation functions are defined:

$$C_{LL}(\mathbf{r}) = \langle u_L(\mathbf{x}) u_L(\mathbf{x} + \mathbf{r}) \rangle, \tag{2.6}$$

$$C_{RR}(\mathbf{r}) = \langle u_R(\mathbf{x}) u_R(\mathbf{x} + \mathbf{r}) \rangle. \tag{2.7}$$

where u_L is the component of the velocity in the longitudinal ($\hat{\mathbf{r}}$) direction, and u_R is the component in the normal direction, perpendicular to $\hat{\mathbf{r}}$.

2.4 Length Scales of Turbulent Motion

Turbulence is generated at large scales, and energy is dissipated away at small scales. Dissipation is the process by which the kinetic energy in the system is converted into heat. The rate at which energy is dissipates is given by ϵ, which is equal to $-\dfrac{dE}{dt}$ in the case where no external forces are present[1]. There are three primary length scales used to characterise turbulent behaviour, which will be discussed below.

Energy enters the system at what is called the **integral length scale**. It is defined by integrating the dimensionless correlation function over all space[1].

$$L = \int_0^\infty \frac{C_{LL}(r)}{u^2} dr = \int_0^\infty f(r) dr. \tag{2.8}$$

As distant velocities should not be correlated, this should always take a finite value. A corresponding time scale, the **large eddy turnover time** denoted by τ, and the characteristic velocity can also be defined. The characteristic velocity is given by the root mean square velocity. Since $E = \frac{1}{2}(u_x^2 + u_y^2 + u_z^2) = \frac{3}{2}u_{rms}^2$ for a homogeneous isotropic system, U and τ are given by

$$U = u_{rms} = \sqrt{\frac{2}{3}E}, \tag{2.9}$$

$$\tau = \frac{L}{U}. \tag{2.10}$$

These are the largest scales of the motion, and are the characteristic length and velocity used in the definition of the Reynolds number (equation 2.3).

The **Kolmogorov microscale** is the length at which turbulent energy is dissipated into heat[1]. This is the smallest scale at which turbulence can occur, before the system is totally governed by the viscosity. By definition, a Reynolds number defined at this scale must equal unity. From this a Kolmogorov velocity scale and a Kolmogorov time scale can be defined.

$$l_D = \left(\frac{\nu^3}{\epsilon}\right)^{\frac{1}{4}}, \tag{2.11}$$

$$u_D = (\nu\epsilon)^{\frac{1}{4}}, \tag{2.12}$$

$$t_D = \frac{l_D}{u_D} = \left(\frac{\nu}{\epsilon}\right)^{\frac{1}{2}}, \tag{2.13}$$

$$Re_D = \frac{u_D l_D}{\nu} = 1. \tag{2.14}$$

where ν is the viscosity and ϵ is the rate of (kinetic) dissipation[2]. In order to study the energy spectrum the reciprocal of the Kolmogorov microscale, the Kolmogorov wavenumber, is defined by

$$k_D = \frac{1}{l_D} = \left(\frac{\epsilon_u}{\nu^3}\right)^{\frac{1}{4}}. \tag{2.15}$$

The **Taylor length scale** is an intermediary length scale, and represents the length at which the viscosity term in the Navier-Stokes equation begins to dominate over the energy mixing term (see equation 2.1, section 2.1)[1]. It is found by Taylor expanding the correlation function (assumed to be even) and evaluating the second term ($f''(r)$ at $r = 0$)[3]. The Taylor length scale can be approximated as

$$\lambda \approx \left(\frac{10\nu k}{\epsilon}\right)^{\frac{1}{2}}. \tag{2.16}$$

[2]In most other texts, the Kolmogorov microscale is denoted by η, or η_D, where the D stands for dissipation. In this report, l_D (or, where appropriate, $1/k_D$) has been chosen so as to avoid confusion with η, the resistivity of the fluid.

[3]Note: the Taylor length scale is not named after the Taylor expansion (Brooke Taylor, 1715) from which it is derived, but after physicist Geoffrey Ingram Taylor who first measured it in 1952.

2.5 Spectral Properties and the Energy Cascade

In Fourier space, the transfer of energy from large scales to small scales is equivalent to energy entering the system at low wavenumbers, and dissipating at high wavenumbers. The non-linearity of the Navier-Stokes equation implies that each point in Fourier space is intrinsically coupled with every other point, which make the concept of determining a spectral dependence of the energy. Kolmogorov aimed to simplify this with his 1941 hypotheses[1, 10].

The first hypothesis states that turbulent motions at length scales much smaller than the integral length scale are independent of the input of energy at the large scales. This means that at small scales, any overall inhomogeneity and anisotropy is lost and the motion becomes locally homogeneous and isotropic. The second hypothesis, which has been used in the definition of the Kolmogorov microscale above, states that motion at these length scales is uniquely determined by ν and ϵ. The consequence of this is that the motion at high wavenumbers, where energy is dissipated, is statistically independent of the motion at low wavenumbers, where energy enters the system. The transfer of energy across these wavenumbers is known as the *spectral energy cascade*.

The **inertial subrange** is defined as the range around the Taylor length scale that is large enough that viscosity has no effect on the motion ($l \gg l_D$), but small enough to be unaffected by the large scale motion of the fluid ($l \ll L$)[10, 1]. In k space, this corresponds to a range $k_f < k < k_D$, where k_f is the largest forced wavenumber. This is illustrated in figure 2.

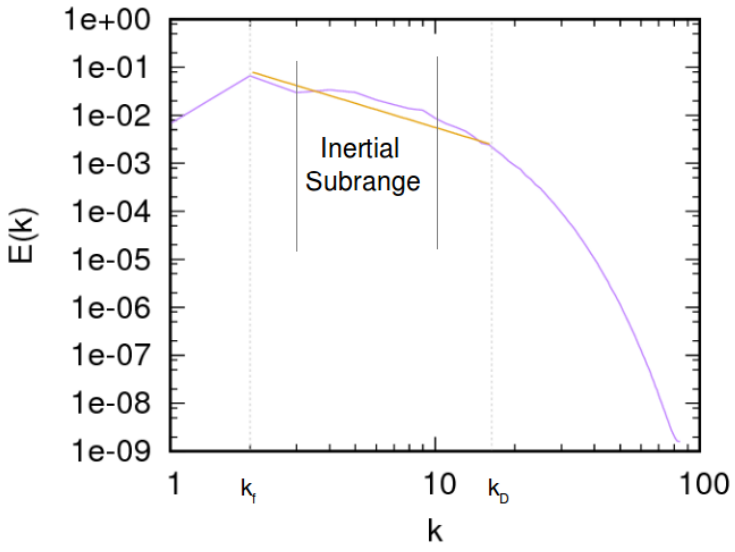

Figure 2. Time averaged kinetic energy spectrum from a stationary simulation (run f1, table 2), shown on a log-log plot. Energy is injected in the range $0 < k \leqslant k_f = 2$, and dissipated at $k > k_D = 16.4$. The behaviour of the spectrum between these values varies with $k^{-5/3}$ as shown by the yellow line.

The energy spectrum describes the amount of energy in each mode, or wavenumber, in Fourier space and is denoted by $E(k)$, where the total kinetic energy is

$$E = \int_0^\infty E(k)dk. \tag{2.17}$$

Kolmogorov's third hypothesis states that within the inertial subrange, the energy spectrum must be independent of both the viscosity, and also of the rate at which energy is put into the system. However, the dissipation rate at each wavenumber in this range (the dissipation rate spectrum), does depend on the viscosity. It can be shown to vary as $\nu k^2 E(k)$, i.e. energy dissipates faster at higher wavenumbers[1]. The total dissipation rate is given by

$$\epsilon = \int_0^\infty 2\nu k^2 E(k)dk. \tag{2.18}$$

Kolmogorov therefore proposed a power law dependence of energy on the wavenumber and dissipation, valid within this range[1, 10]. The wavenumber has dimensions of inverse length, so the energy (per unit mass) in any one mode has units $[E][k^{-1}] = [L^3][T^{-2}]$, and dissipation has units $[L^2][T^{-3}]$. By dimensional analysis, one arrives at Kolmogorov's $\frac{5}{3}$ law for the energy spectrum:

$$E(k) = C\epsilon^{\frac{2}{3}}k^{-\frac{5}{3}} \tag{2.19}$$

where ϵ is the rate of dissipation per unit mass and k is the wavenumber. This can be seen in figure 2.

3 Magnetohydrodynamics

3.1 Introduction to Magnetohydrodynamics

In this section, the hydrodynamic turbulence theory is modified to include conducting fluids. To distinguish the terms defined in the previous section for the kinetic field from their magnetic counterparts, indeces u and b have been used to refer to the kinetic and magnetic fields respectively.

In non-conducting fluids, viscosity is the measure of how 'easily' the fluid flows in response to a change in the force. A highly viscous substance will not respond to a force as readily as a more mobile one. The electromagnetic equivalent of this is the resistivity, which measures how 'easily' the current flows in response to a change in the magnetic field. This allows us to define the **magnetic Reynolds number** using the characteristic velocity and length scales from before (section 2.1)[2, 11]:

$$Re_M = \frac{UL}{\eta}. \tag{3.1}$$

As in section 2.1, the fluid is assumed to be incompressible, to give a divergenceless velocity field. The magnetic field, however, is inherently divergenceless so no further assumptions need to be made.

$$\boldsymbol{\nabla} \cdot \mathbf{u} = 0, \tag{3.2}$$

$$\boldsymbol{\nabla} \cdot \mathbf{b} = 0. \tag{3.3}$$

Combining the Navier-Stokes equations for fluid flow with Maxwell's equations, which dictate how the fluid will respond to a changing magnetic field, one can derive the **MHD Equations**[2]:

$$\frac{\partial \mathbf{u}}{\partial t} + (\mathbf{u} \cdot \boldsymbol{\nabla})\mathbf{u} = -\frac{1}{\rho}\boldsymbol{\nabla} P + \frac{1}{\rho}(\boldsymbol{\nabla} \times \mathbf{b}) \times \mathbf{b} + \nu \nabla^2 \mathbf{u} + \mathbf{F_u}, \tag{3.4}$$

$$\frac{\partial \mathbf{b}}{\partial t} + (\mathbf{u} \cdot \boldsymbol{\nabla})\mathbf{b} = (\mathbf{b} \cdot \nabla)\mathbf{u} + \eta \nabla^2 \mathbf{b} + \mathbf{F_b}. \tag{3.5}$$

The first equation, which describes the changes in the velocity field over time, is very similar to the Navier-Stokes equation (section 2.1, equation 2.1), but with the addition of a kinetic forcing term, the *Lorentz force*, which is due to the magnetic field. The second is an analogous equation for the change in the magnetic field over time, where the resistivity has replaced the viscosity in the ∇^2 term, and the energy mixing term is expressed slightly differently. The last term in each equation is an optional forcing term. For decaying turbulence (section 5.1), both forcing terms are omitted, and for the stationary simulations (section 5.2) in this project, only kinetic forcing ($\mathbf{F_u}$) has been used, and $\mathbf{F_b} = 0$.

The **magnetic Prandtl number** is the dimensionless ratio of the viscosity to the resistivity[2]:

$$Pr_m = \frac{\nu}{\eta} = \frac{Re_m}{Re} \tag{3.6}$$

which is qualitatively a ratio of the amounts of turbulent motion in each field. Currently, most research has focused on Prandtl numbers $\simeq 1$, as these are the most straightforward to simulate. This is because at $Pr_m \simeq 1$, the length scales of the kinetic turbulence and the magnetic turbulence are similar. However, as mentioned in section 1, many physical situations of interest have Prandtl numbers much larger or much smaller than 1, so the focus of this project has been on varying the Prandtl number away from unity.

3.2 Ideal MHD and Conserved Quantities

Ideal turbulence is a theoretical concept derived in the limit of vanishing viscosity, where the Reynolds number is infinite. Equivalently, ideal MHD is the limit of vanishing resistivity, or infinite magnetic Reynolds number. Although the results in this report are for finite ν and η, this section is included for completeness, as certain quantities pertaining to MHD are more readily understood in this limit. Due to the absence of viscosity and resistivity, no energy is dissipated into heat, and dissipation vanishes. Therefore, although energy is transferred between kinetic and magnetic fields, the total energy is conserved in the ideal system[12].

Other quantities associated with the behaviour of the fluid are the kinetic helicity (H_K), the magnetic helicity (H_M), and the cross helicity (H_C). Helicity is a measure of the 'twistedness' of the kinetic/magnetic field[12], or, in the case of cross-helicity, the linkage between kinetic and magnetic fields[13]. These terms are defined as:

$$H_K = \int_V (\mathbf{u} \cdot \boldsymbol{\omega}) dV, \tag{3.7}$$

$$H_M = \int_V (\mathbf{a} \cdot \mathbf{b}) dV, \tag{3.8}$$

$$H_C = \int_V (\mathbf{u} \cdot \mathbf{b}) dV, \tag{3.9}$$

where $\boldsymbol{\omega}$ in equation 3.7 is the vorticity $\boldsymbol{\omega} = \boldsymbol{\nabla} \times \mathbf{u}$ (section 2.1) and $\mathbf{a}$ in equation 3.8 is the vector potential for the magnetic field, $\mathbf{b} = \boldsymbol{\nabla} \times \mathbf{a}$[12, 13, 2].

In ideal hydrodynamic turbulence, kinetic helicity is conserved in the absence of a magnetic field[12]. However, the addition of the magnetic forcing terms in the equation for $\dfrac{\partial \mathbf{u}}{\partial t}$ (equation 3.4), mean H_K is not conserved in ideal MHD. Magnetic and cross helicity on the other hand, are conserved. This can be seen by substituting equations 3.4 and 3.5 into equations 3.8 and 3.9 and taking the time derivative. The resulting terms are

$$\frac{dH_M}{dt} = -(\nu + \eta) \int_V (\mathbf{j} \cdot \boldsymbol{\omega}) dV, \tag{3.10}$$

$$\frac{dH_C}{dt} = -\eta \int_V (\mathbf{j} \cdot \mathbf{b}) dV \tag{3.11}$$

where $\mathbf{j} = \boldsymbol{\nabla} \times \mathbf{b}$ is the current density[2]. Similarly, by taking the time derivative of the total energy,

$$E_T = \int_V (\mathbf{u}^2 + \mathbf{b}^2) dV, \tag{3.12}$$

one obtains

$$\frac{dE_T}{dt} = -\eta \int_V \mathbf{j}^2 dV - \nu \int_V \omega^2 dV. \tag{3.13}$$

In the ideal limit $\eta = \nu = 0$, it is clear to see that $\dfrac{dH_M}{dt}$, $\dfrac{dH_C}{dt}$ and $\dfrac{dE_T}{dt}$ vanish. H_M, H_C, and E_T are therefore conserved in ideal MHD and are called *ideal invariants*.

3.3 Statistical Approach to MHD

To extend the statistical formulation given in section 2.2 the magnetic field must also be decomposed as $\mathbf{B} = \bar{\mathbf{B}} + \mathbf{b}$, where $\bar{\mathbf{B}}$ is the mean value of $\mathbf{B}$ and $\mathbf{b}$ are fluctuations on the mean, so $\langle \mathbf{b} \rangle = 0$. In order to achieve a system which is both homogeneous and isotropic, both the average magnetic field and the average kinetic field must be zero:

$$\bar{\mathbf{B}} = 0 \qquad\qquad \bar{\mathbf{U}} = 0. \tag{3.14}$$

Since these flow perpendicular to each other, we cannot transform a system with a net velocity field into a frame where both fields are stationary. The study of homogeneous isotropic MHD is therefore purely a theoretical one, but allows the study of the fundamental properties of MHD turbulence.

3.4 Length Scales of MHD

Just as for non-conducting turbulence, analogous characteristic length, time, and velocity scales can be defined for MHD turbulence. Redefining the integral length scale of the kinetic field as

$$L_u = \int_0^\infty \frac{C_{LL}^{uu}(r)}{u^2} dr \tag{3.15}$$

where C_{LL}^{uu} is the correlation tensor between the kinetic field and itself, the magnetic integral length scale can then be defined as

$$L_b = \int_0^\infty \frac{C_{LL}^{bb}(r)}{b^2} dr. \tag{3.16}$$

C_{LL}^{bb} is the correlation tensor between the magnetic field and itself[14].

Similarly a magneto-resistive microscale, and its reciprocal wavenumber, can be defined as

$$l_D^b = \left(\frac{\eta^3}{\epsilon_b}\right)^{\frac{1}{4}}, \tag{3.17}$$

$$k_D^b = \frac{1}{l_D} = \left(\frac{\epsilon_b}{\eta^3}\right)^{\frac{1}{4}} \tag{3.18}$$

where the resistivity η has been used as an analogous quantity to the viscosity, and ϵ_b is the magnetic dissipation rate. At this scale, energy in the turbulent magnetic field is dissipated into heat via the resistivity.

For $Pr_m = 1$, the magnetic length length scales will be equal to their kinetic counterparts. However, away from unity, the ratio of magnetic dissipative length to the kinetic dissipative length scale (the Kolmogorov microscale) varies with magnetic Prantl number, $\frac{l_D^b}{l_D^u} \sim Pr_m^{0.5}$[15]. For $Pr_m > 1$, this gives rise to the the subviscous range, the range between the magnetic dissipative length and the Kolmogorov microscale ($l_D^b < l < l_D^u$).

3.5 Energy Cascade and Dynamo Action in MHD

In hydrodynamic turbulence, there is a *direct* cascade of kinetic energy from larger scales down to smaller scales, where it is dissipated into heat (section 2.4). This direct cascade is also seen in the magnetic energy, as one would expect. However, not all measured quantities behave in this manner, and the magnetic helicity (equation 3.8) exhibits an *inverse* cascade[13]. This is where helicity is transferred from small scales up to larger scales, or high wavenumbers to low wavenumbers.

Examining ideal MHD, it can be shown that the magnetic and kinetic energy, and the cross helicity, all of which exhibit direct cascades, peak at high wavenumbers, while the magnetic helicity peaks at small wavenumbers[2]. This peak of H_M at low k can help explain the reason for this inverse cascade. Tthe dynamics of the system will tend towards their ideal limit as the system progresses, and thus the spectral magnetic helicity will move from high wavenumbers down to lower ones[2].

Dynamo theory describes how turbulence in the magnetic field is sustained over time by turbulence in the kinetic field, and is thought to explain the magnetic field generated by the Earth's core. A small scale dynamo occurs when energy is transferred to the magnetic field at small scales (high k), through a linear process that transfers energy proportional to a $k^{3/2}$ spectrum[16]. Although this process is derived by assuming an idealised turbulent system at very large ($\gg 1$) Pr_m and is due to the large viscous subrange present[15], it has been shown to apply to systems where Pr_m is close to 1, as in this report[17, 5].

Non-linear large scale dynamos transfer energy to the magnetic field at scales larger than the scale at which the energy is put into the system[16], which relies on the inverse cascade of helicity to excite the larger scales of the motion. The simulations performed in this study, however, are non-helical, and thus exhibit small scale dynamo action only.

4 Direct Numerical Simulations

Many methods are currently used to investigate fluid dynamics and turbulence, both with and without MHD effects. These include Larger Eddy Simulations (LES), Reynolds Averaged Navier-Stokes (RANS), and Direct Numerical Simulation (DNS). As with all numerical simulations, choosing the right method involves an exchange between accuracy and computation time. RANS and LES methods are less computationally expensive than DNS, but focus on the large scales of the motion.

For our purposes, DNS is the optimal method as it captures all the length scales of the fluid right down to the Kolmogorov length scale, thus modelling the turbulence exactly (which is discussed further in section 4.1)[1, 2]. The trade-off for this level of accuracy is the amount of memory needed and large computational cost, which scales as $\sim Re^3$ for hydrodynamic turbulence[1].

4.1 Resolution

The phenomenon of turbulence involves many different length scales(sections 2.4 and 3.4), which can be problematic when simulating turbulent fluids numerically. A lattice spacing that is larger than the Kolmogorov microscale would mean energy dissipation could not accurately be measured. Similarly, a box size not significantly larger than the integral length scale would fail to capture all the dynamics needed to accurately simulate the turbulence in the first place.

A fully resolved simulation captures the dynamics at the smallest of length scales, but will require a very large lattice at high magnetic and kinetic Reynolds number, as an increase in Reynolds number incurs a shortening of the Kolmogorov microscale. Since the calculation are primarily in Fourier space, to capture all dynamics a simulation must have modes greater than the Kolmogorov wavenumber, k_D, for both the magnetic and kinetic fields.

Since each simulation is run in a box with sides of length 2π and periodic boundary conditions, the maximum value for k is given by

$$k_{max} = \frac{N}{2\pi} \tag{4.1}$$

where N is the number of collocation points, or lattice points, that make up the mesh.

A simulation is considered fully resolved when $\frac{k_{max}}{k_D} \geqslant 1.25$ ($k_{max} l_D \geqslant 1.25$), and partially resolved when $\frac{k_{max}}{k_D} \geqslant 1$ ($k_{max} l_D \geqslant 1$). This applies to both the kinetic and magnetic fields, for their respective microscales. At $Pr_m = 1$, both of these scales will be equal, but at Pr_m away from 1 it becomes challenging to fully resolve both length scales. Further discussion on this is presented in section 5.1.

4.2 DNS2012

The code used in this project is called DNS2012 and was written by Dr. Yoffe in 2012 for hydrodynamic turbulence[3], and extended to MHD by Dr. Linkmann in 2015[14]. This code has been extensively tested in these sources for both hydrodynamic and MHD turbulence.

Both the velocity and magnetic field need to be initialised before the simulation can begin. This is done by generating a random Gaussian field in configuration space, which will not necessarily represent a solution to the MHD equations. These are Fourier transformed to set initial helicities according the input conditions, although helicity has been set to 0 for this project. Both fields are then normalised by the desired initial energy spectrum.

Since MHD is described by coupled partial differential equations, Fourier analysis methods are very effective for evolving the spatial parts, as these transform to linear ordinary differential equations in Fourier space. However, the non-linear multiplication terms in equations

3.4 and 3.5 transform to convolutions in Fourier space, so these parts are computed in configuration space (i.e. position/coordinate space). Fast Fourier Transforms (FFTs) are used to switch between configuration and Fourier space. This method of numerical simulation is known as *pseudospectral* (where *spectral* methods refers to calculations done entirely in Fourier space). The equations are evolved in time using Heun's Method (a more accurate version of Euler's method[18]). A full description of this method is detailed in [3].

4.3 Forcing Regimes

If no energy is put into the system, energy dissipates via the viscosity and the resistivity and the turbulence decays. To maintain stationary turbulence over a sustained period of time, a forcing regime must be implemented. The forcing used throughout this project was a negative damping kinetic forcing regime given by

$$\mathbf{f}_u(\mathbf{k},t) = \begin{cases} \left(\frac{\epsilon_W}{2E_f}\right)\hat{\mathbf{u}}(\mathbf{k},t) & 0 < |\mathbf{k}| \leqslant k_f \\ 0 & \text{otherwise} \end{cases} \tag{4.2}$$

in spectral space, where $0 < |\mathbf{k}| \leqslant k_f$ is the range of forced modes, ϵ_W is the rate of input of energy, and $\hat{\mathbf{u}}(\mathbf{k},t)$ is the Fourier transformed velocity, scaled to unity[3]. E_f is the total energy contained in the forced modes, i.e. the integral of the energy spectrum from 0 up to k_f. The maximum forced wavenumber, k_f, is typically chosen to be quite low so that the forcing is restricted to the larger scales of the motion.

Choosing ϵ_W is a bit more involved, as a balance must be maintained between the rate of forcing and the timestep of the simulation or the simulation will blow up. Equally, too low a rate of forcing will not be enough to sustain the turbulent motion. To obtain the desired balance, ϵ_W must be such that $\frac{dE_u}{dt} = \epsilon_W - \epsilon_T = 0$ and the total energy remains constant ($\epsilon_T = \epsilon_u + \epsilon_b$).

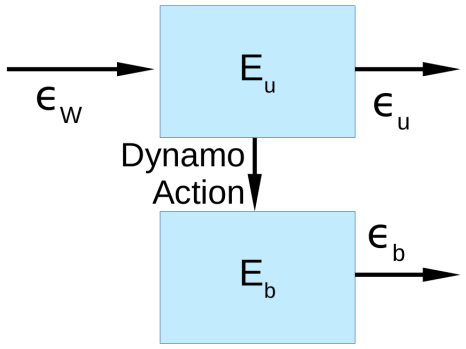

Figure 3. Diagram adapted from sketch in Brandeburg et al., 2014[5].

A simplified description of this process is illustrated in figure 3. Energy enters the kinetic field at low wavenumbers at a rate ϵ_W and is dissipated away at high wavenumbers at a rate ϵ_u, via the self-organisation of the kinetic field. Although the magnetic field is unforced, energy enters the magnetic field by the processes of dynamo action described in section 3.5. This energy is then dissipated at a rate ϵ_b.

In the stationary simulations in this project (section 5.2), k_f was set to 2 and the rate of input of energy, ϵ_W, set to 0.1. These parameters were chosen based on calculated estimates, and test simulations were performed and checked to ensure validity of the data.

4.4 Parallelisation

Parallelisation of computer simulations involves the splitting of calculations into multiple processes that can be computed simultaneously, thus improving computation time. The code used has been parallelised, not only to speed up computation time, but also because the memory needed to store the kinetic and magnetic fields at any snapshot in time is very large, so splitting the amount of data stored at each timestep is desirable.

Each vector field requires 24 bytes per grid point[3], so for a $N = 512$ lattice, the memory required for each field is $N^3 \times 24$ bytes $\simeq$ 3GB, and multiple vector fields must be stored at each time step. The DNS2012 code has been designed to be run on both `eddie` (compute cluster run by the *Edinburgh Compute and Data Facility*) and `archer` (the supercomputer run by the *Edinburgh Parallel Computing Centre*)[3].

This has been done using 1-dimensional data decomposition, which is optimal for the ranges of N lattice points in this project. Data is split into N_p sections along the x axis, where N_p is the number of processes. It is important to note that because of this, the number of lattice points, N, must be chosen to be a multiple of the number of processes so that $\frac{N}{N_p}$ gives a positive integer value. For this reason, N is always chosen so that $N = 2^n$ and $N_p = 2^m$ where n, m are positive integers and $m < n$.

4.5 Running the Code

The parameters of the simulations, such as the Prandtl number, the viscosity, the total run time (in simulation time units), and the type of forcing (if used) are specified in an input file. The initial helicity (section 3.2) can also be set, although this was left as 0 for the simulations in this project, as the focus was on non-helical turbulence. For forced simulations, the forcing parameters, ϵ_W and k_f are also specified here.

Computational parameters, such as the number of processors, path to input file, output file names, the length of time to run the simulation (in real time units) and how often to create checkpoint backups are specified in the job script. When using `archer`, the number of nodes

used must also be specified here, and must be large enough to contain the specified number of processors.

The code also allows for checkpoint saving; snapshots of the velocity and magnetic field can be taken at a certain time, specified in the input file in units of real time (as opposed to the time units used in the simulation) and simulations restarted from this point. This is often necessary, as simulations can take well over 24 hours to run. This checkpoint saving also allows visualisations of the simulations to be realised at this time.

4.6 Post-processing

A number of post-processing scripts were used to calculate the derived quantities that characterise the flow. Values for the total magnetic and kinetic energy and dissipation as a function of time are found by integrating their respective spectra over all possible values of k at each time step. Integral lengths are found by evaluating equations 3.15 and 3.16 and the r.m.s. velocity (equation 3.1) can be calculated from the kinetic energy (equation 2.9).

For decaying simulations, scripts were written to find the peak of dissipation and extract the relevant spectral data. For stationary simulations, time averaged values spectral data was calculated. The Reynolds numbers Re and Re_m, and the Kolmogorov microscales l_D^u and l_D^b are then calculated from these derived quantities, combined with the parameters from the input file.

5 Results and Discussion

Without the use of any forcing, all energy is dissipated and there ceases to be any turbulent motion. However, by studying the turbulence as it begins to decay, many interesting results can still be found. Simulations of turbulent motion that have been allowed to dissipate away in this manner will be referred to as *decaying simulations*.

In order to maintain turbulent behaviour over sustained time periods, a forcing regime must be implemented (section 4.3). Simulations that have been forced, and reach a stationary state will be referred to as *stationary simulations*. As the focus is on trends in the data as opposed to the actual values, and Pr_m, Re and Re_m are dimensionless, all units are simulation units unless specifically stated.

5.1 Decaying Simulations

Various decaying simulations were performed on different lattice sizes (128^3, 512^3, and 1024^3), at Prandtl numbers between 0.1 and 10. A list of the different decaying simulations run can be seen in table 1. Simulations were run for 10 units of time, with a timestep of 0.001,

Run	N	Pr_m	ν	η	Re	Re_m	$k_{max}l_D^u$	$k_{max}l_D^b$
An128	128	1	0.001	0.001	149.81	149.81	0.310	0.299
An*	512	1	0.001	0.001	171.60	171.60	1.278	1.139
An1024*	1024	1	0.001	0.001	167.89	167.89	2.560	2.279
Bn128	128	10	0.01	0.001	21.049	210.49	1.434	0.345
Bn*	512	10	0.01	0.001	21.446	214.46	6.006	1.371
Bn1024*	1024	10	0.01	0.001	21.135	211.35	11.992	2.768
[Cn	512	0.1	0.001	0.01	200.216	20.022	1.561	5.758]

Table 1. List of decaying simulations performed. The Reynolds number and Kolmogorov microscale were calculated from measurements of $\langle U \rangle$, L, ϵ_{kin}, ϵ_{mag} taken at the peak of dissipation. The bracketed run, Cn, was run for completeness when analysing Pr_m dependence. It was run at a later date and thus is not present in the analysis of the resolution in this section. Simulations with a * were run by Mairi McKay

which was sufficient time for the energy and the rate of dissipation of energy to decay away. Simulations with a grid size of 512^3 or 1024^3 were run on `archer`, and simulations with a grid size of 128^3 were run on `eddie`.

Running simulations with the same input conditions on different lattice sizes meant that simulations that were fully resolved could be directly compared with under resolved simulations and the effects of poor resolution investigated. Measurements were taken at the time of peak dissipation, which is common practice in simulations of decaying turbulence [4, 19, 20, 3]. For Prandtl numbers not equal to one, the peak of magnetic and kinetic dissipation do not have to occur at the same time. The time used was that of the peak that occurred later, as was done in Sahoo et al., 2011[4].

As seen in table 1, the simulations for a lattice of 128 are severely under-resolved, except in the case of the kinetic field with $Pr_m = 10$. This is due to the lower viscosity (and thus lower Reynolds number) used to obtain the higher Prandtl number. The resolution is examined further in figure 4, where a normalised cumulative spectrum has been graphed over the ratio of k to k_D. Values for the energy/dissipation at a given k represent the fraction of the total energy/dissipation contained in modes $\leqslant k$, and the k axis has been normalised by a factor of k_D. In a continuous space, these quantities are integrals over k given by:

$$E^{u/b}_{\text{cumulative}}(k) = \int_0^k E_{u/b}(k')dk' \tag{5.1}$$

$$\epsilon^{u}_{\text{cumulative}}(k) = \int_0^k 2\nu k^2 E_u(k')dk' \tag{5.2}$$

$$\epsilon^{b}_{\text{cumulative}}(k) = \int_0^k 2\eta k^2 E_b(k')dk' \tag{5.3}$$

where the total energy/dissipation is the integral over all k-space (see equations 2.17 and 2.18).

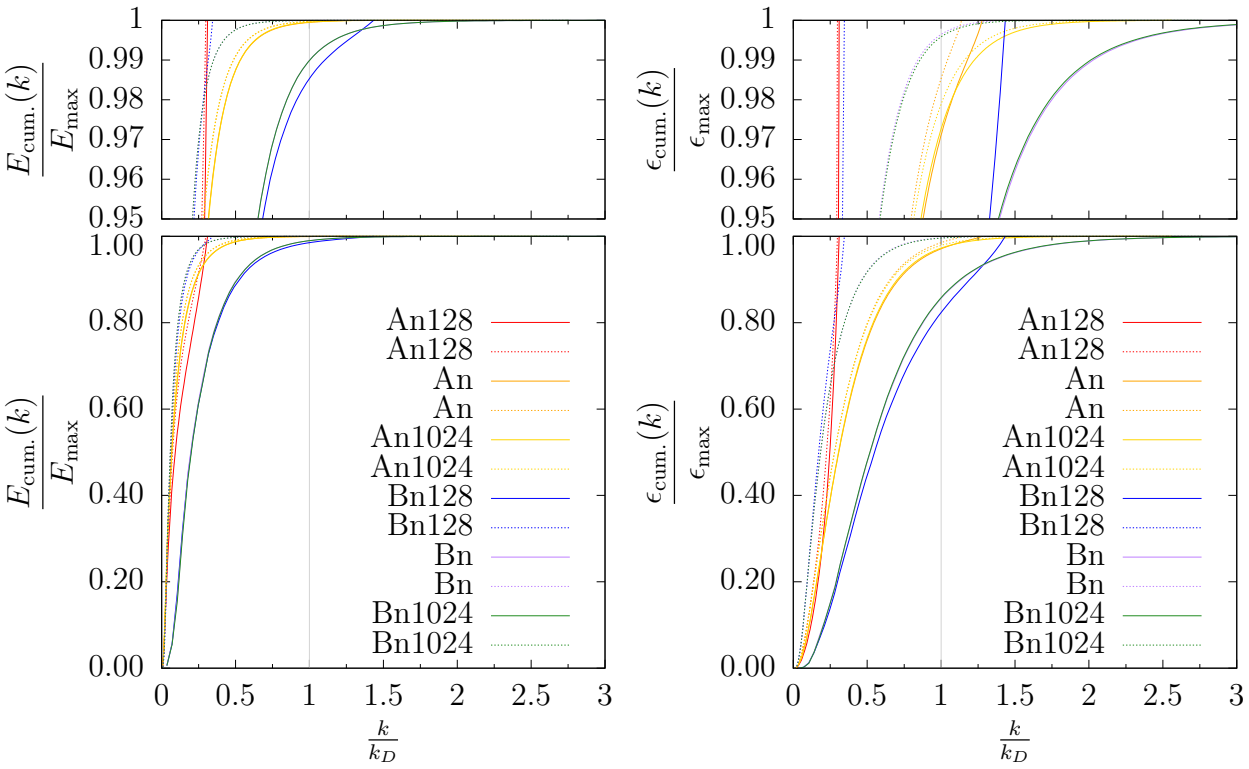

(a) (b)

Figure 4. Location of the energy (a) and dissipation (b) as a fraction of the total contained in modes $\leq k$. The solid lines represent the kinetic energy/dissipation, and the dashed lines the magnetic energy/dissipation. The top section focuses on the resolution needed to capture 95% of the dynamics.

In figures 4(a) and (b), some values for energy and dissipation respectively can be seen to shoot off the top of the graph, implying information is lost. For the fully resolved simulations ($N = 1024$) there is a smooth accumulation to higher values of k. For the simulations run on a 512 lattice, figure 4(a) shows a smooth accumulation to higher k, implying that the energy has been fully captured at all scales, but upon close inspection of figure 4(b) a loss in accuracy of dissipation can be seen in the orange curve, where $Pr_m = 1$ and $N = 512$. From this it can be seen that fully resolved simulations ($k_{max} l_D \geqslant 1.25$) do capture $> 99\%$ of the energy, but to capture all of the dissipative dynamics higher $k_{max} l_D$ is needed.

The effects of this can be seen in figures 5 and 6. The curves for the 512 and 1024 simulations are very similar, but the loss of resolution for the 128 simulation causes a disparity in the results. In figure 5, it can be seen that the kinetic energy decays away quickly, but a peak can be seen in the magnetic energy at $t \simeq 0.3$. This due to the small scale dynamo effect (section 3.5). This peak is absent for $Pr_m = 0.1$, as the Prandtl number is too low for the dynamo to be excited.

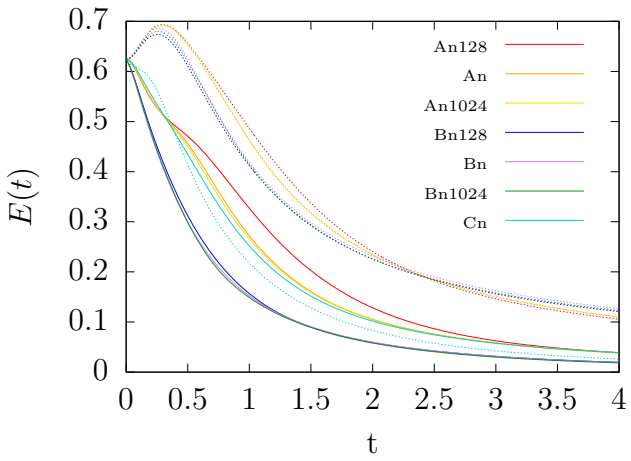

Figure 5. Energy time graph for decaying turbulence, where the solid line is the kinetic energy and the dashed line is the magnetic energy

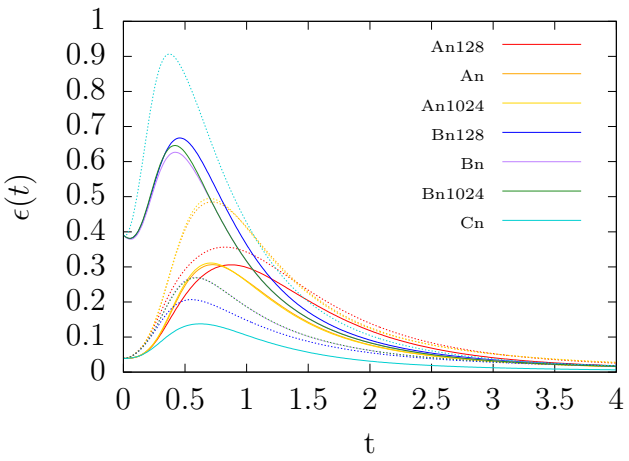

Figure 6. Dissipation time graph for decaying turbulence, where the solid line is the kinetic dissipation rate and the dashed line is the magnetic dissipation rate

This is further illustrated in figure 6, where a large peak is seen in the magnetic dissipation rate for $Pr_m = 0.1$ as the field is not being sustained by the dynamo. This peak occurs before the peak in kinetic dissipation. For $Pr_m \geqslant 1$ the dynamo has been excited, and for both $Pr_m = 1$ and $Pr_m = 10$ the peak of magnetic dissipation is much less pronounced, and occurs after the peak of kinetic dissipation. The magnetic energy is dissipating away out of the system at a much slower rate as it is being sustained due to the small scale dynamo effect.

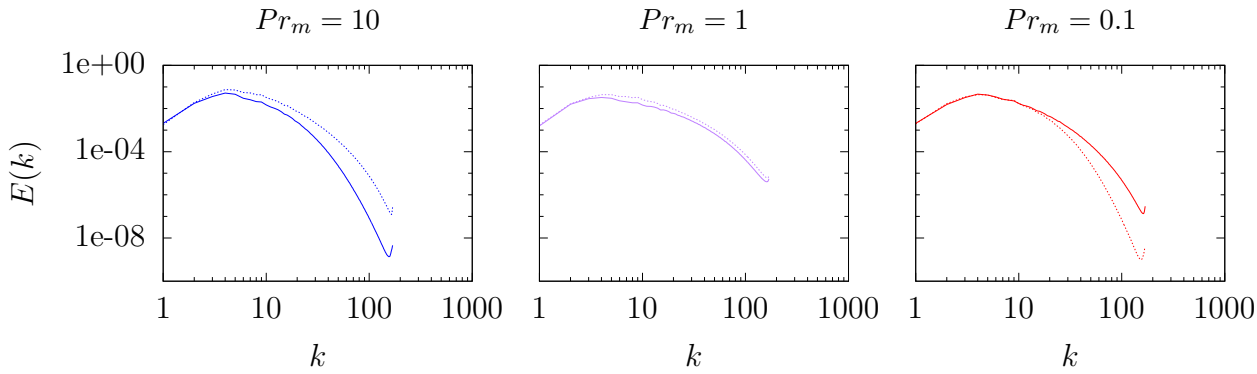

Figure 7. Log-log plots of energy spectra at peak of dissipation for decaying turbulence, where the solid line represents the kinetic energy and the dashed line the magnetic energy. $Pr_m = 10$ on the left, $Pr_m = 1$ for the centre graph, and $Pr_m = 0.1$ on the right.

The energy spectra seen in figure 7 from the peak of dissipation illustrate the transfer of energy from kinetic to magnetic with increasing k. At higher k more energy is transferred

to $E_b(k)$ as we increase Pr_m from 0.1 to 10. This is as expected from results in Sahoo et al.[4] for decaying turbulence measured at the peak of dissipation.

In figure 8(a) the ratio of magnetic to kinetic energy for $Pr_m \geqslant 1$ can be seen to increase with time. In addition, the rate at which this occurs increases with increasing Prandtl number. This is in agreement with Sahoo et al.[4] in which a similar trend can be seen for decaying simulations. In their results this trend extended to $Pr_m < 1$, where there was also an increase, albeit a smaller one for $Pr_m = 0.1$. However, these results show a decrease in $\frac{E_b}{E_u}$ for $Pr_m = 0.1$. In [4], resistivity was kept fixed, and viscosity was varied to obtain different Prandtl numbers. In the simulations in this report, resistivity was varied for simulations with $Pr_m < 1$ and viscosity varied for simulations with $Pr_m > 1$. Since it is hypothesised that this ratio is dependent on the magnetic Reynolds number and not the Prandtl number (discussed further in section 5.3), this would explain these results.

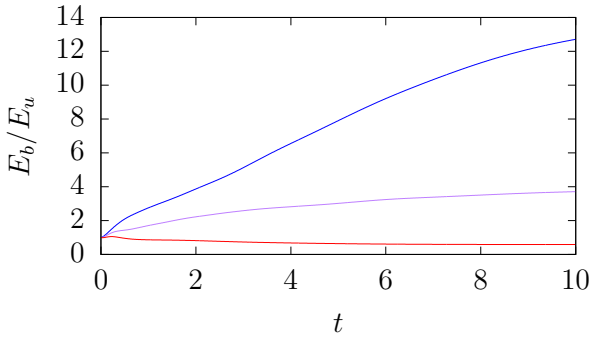

(a)

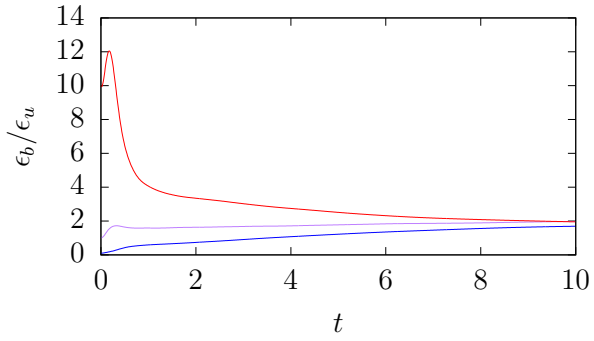

(b)

Figure 8. Ratio of magnetic to kinetic energy (a), and magnetic to kinetic dissipation (b), where $Pr_m = 10$ is in blue, $Pr_m = 1$ is in purple and $Pr_m = 0.1$ is in red.

5.2 Stationary Simulations

Run	Pr_m	ν	η	Re	Re_m	$k_{max}l_D^u$	$k_{max}l_D^b$
f7	0.125	0.00125	0.01	592.446	74.056	1.111	6.152
f6	0.25	0.0025	0.01	327.290	81.823	1.993	5.621
f5	0.5	0.005	0.01	165.295	82.648	3.097	6.501
f1	1	0.01	0.01	87.347	87.347	5.136	6.807
f2	2	0.01	0.005	85.418	170.836	5.522	3.461
f3	4	0.01	0.0025	80.114	320.456	5.762	1.951
f4	8	0.01	0.00125	87.187	697.497	5.706	1.162

Table 2. List of stationary simulations performed. Measurements of the Reynolds number and Kolmogorov microscale calculated from time averaged values of $\langle U \rangle$, L, ϵ_{kin}, ϵ_{mag}. All simulations were run with a box size of 256^3

Seven stationary simulations were run with Prandtl number ranging from $1/8 \leqslant Pr_m \leqslant 8$, detailed in table 2. These simulations were performed on a $N = 256$ lattice for a duration of 50 units of time, with a timestep of 0.001. This was a sufficient length of time to allow the initial conditions decay away, and then for the forcing to take effect over a long enough time to take time averaged measurements of the quantities (rather than taking measurements at the peak of dissipation).

The method by which the system is forced is detailed in section 4.5. Energy was put into the system at a rate of 0.1 for wavenumbers up to $k_f = 2$. These simulations were run on `eddie`, and made use of the checkpoint saving[3, 14] to allow them to run over multiple days.

Ideally, these simulations would have been run with $N = 512$ to get the resolutions seen in the decaying case, but due to the longer length of time required to run stationary simulations this was not feasible. Instead, an $N = 256$ lattice was chosen, and viscosity increased to 0.01, the highest value it can take while still exhibiting some turbulent behaviour. The range of Prandtl numbers studied was reduced to $1/8 \leqslant Pr_m \leqslant 8$, where the $Pr_m = 1/8$ and $Pr_m = 8$ runs are only partially resolved ($1 < k_{max}l_D < 1.25$) for either the kinetic or magnetic field, as shown in table 2.

Figures 9, 10 and 11 show the time averaged energy spectra for the stationary simulations. Just as in the decaying case, kinetic and magnetic energy have roughly the same spectra for $Pr_m = 1$. At high k, there is more magnetic energy present for $Pr_m > 1$, and more kinetic energy present for $Pr_m < 1$. This is in agreement with results in Sahoo et al.[4], where viscosity was kept fixed, and resistivity varied for both $Pr_m < 1$ and $Pr_m > 1$. There is also agreement with results in Brandenburg et al. 2011[8], although these were obtained using helical forcing.

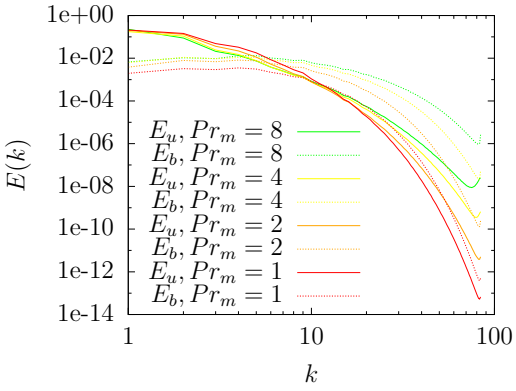

Figure 9. Log-log plot of energy spectra for $Pr_m \geqslant 1$

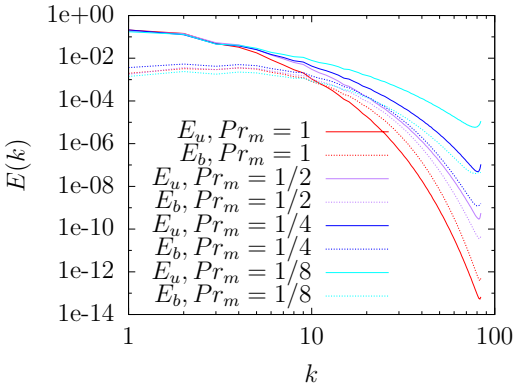

Figure 10. Log-log plot of energy spectra for $Pr_m \leqslant 1$

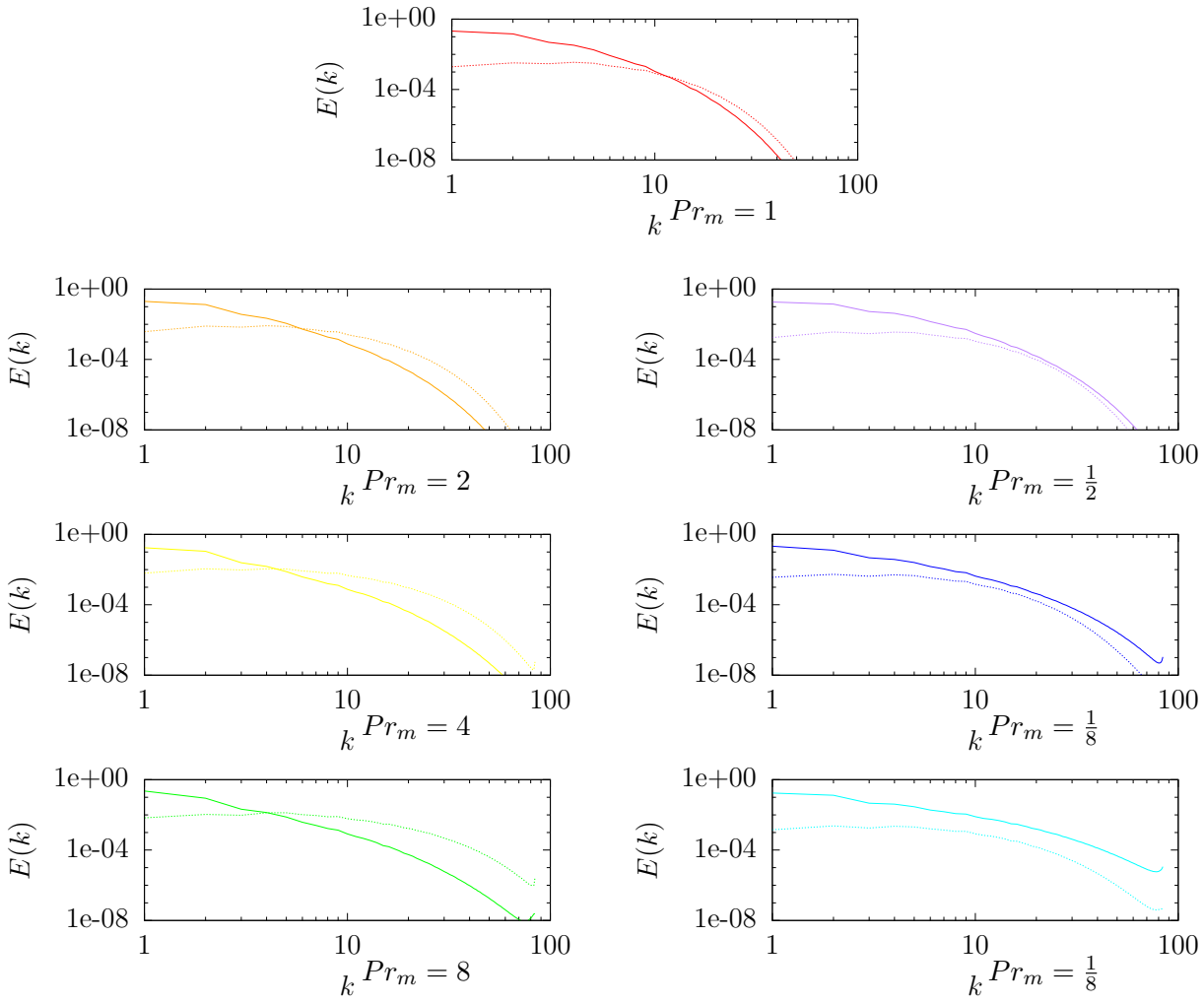

Figure 11. Log-log plots of energy spectra for $Pr_m = 1$ on top, $Pr_m > 1$ on the left, and $Pr_m < 1$ on the right. Solid lines represent kinetic energy spectra and dashed lines represent magnetic energy spectra.

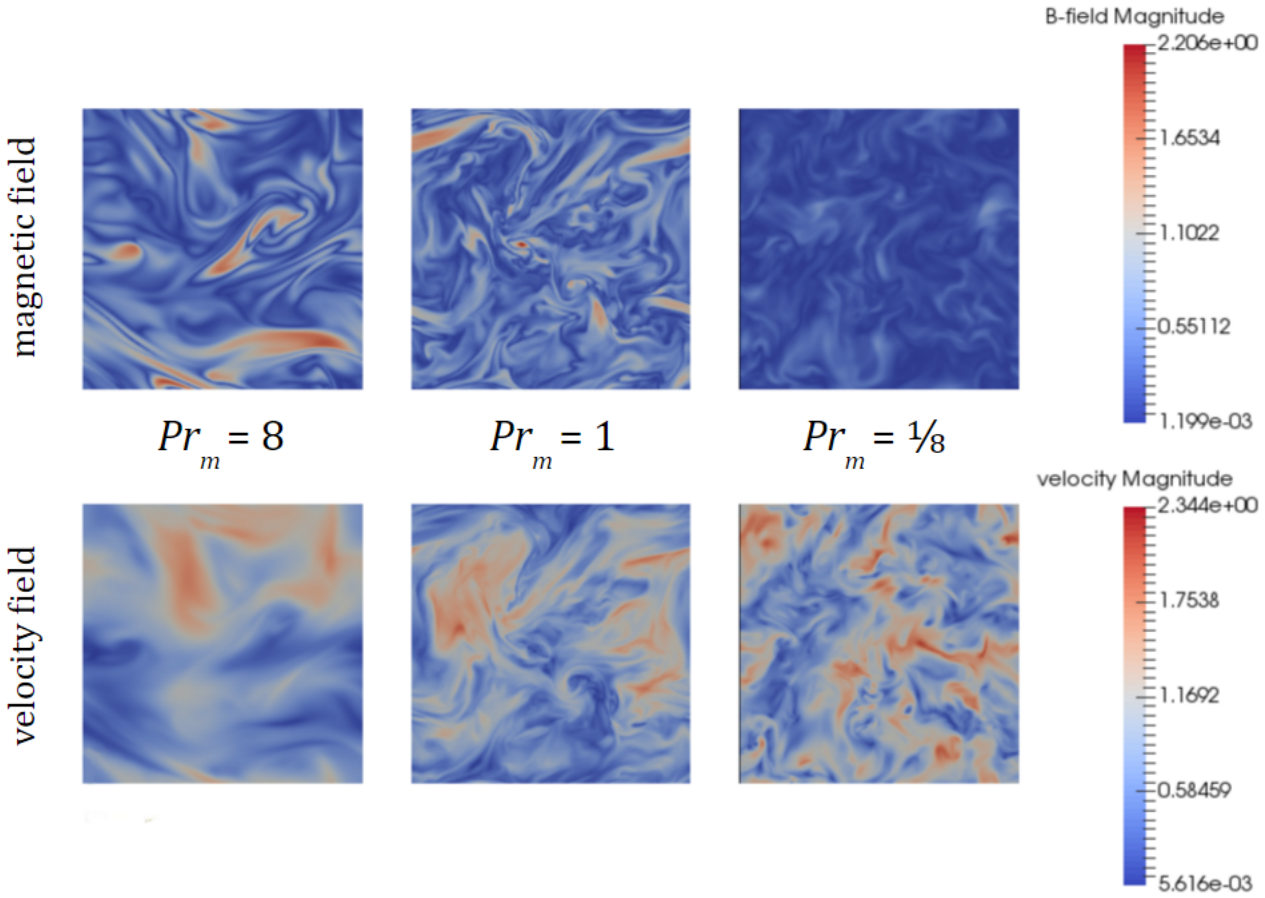

Figure 12. visualisations of simulations f3, f1, and f7 from table 2. These are 2D slices in the y-z plane from the centre of the 3D lattice. They have been taking from an arbitrary point in time after the stationary state has been reached, that is representative of the behaviour

A visualisation of the fields in figure 12 has been included to compare the levels of turbulence present in the kinetic and magnetic fields at different kinetic and magnetic Reynolds numbers. At $Pr_m = 1$, both fields exhibit comparable amounts of turbulent motion. Higher values for Re_m than Re were obtained for $Pr_m > 1$ as a result of varying η while keeping ν fixed. This corresponds to a relatively smooth kinetic field for $Pr_m = 8$, and a more turbulent magnetic field. Similarly, as ν was varied while keeping η fixed for $Pr_m < 1$, more turbulent behaviour can be seen in the kinetic field for $Pr_m = 1/8$ than the magnetic field.

Figure 13 examines the energy and dissipation over time after the passing of 20 units of time, after which the initial conditions have decayed away and the simulation is considered to be statistically steady. For $Pr_m \geqslant 1$ The spacing between the magnetic and kinetic energy in figure 13(a) can be seen to increase with decreasing Prandtl number, and is further by the ratios in 14(a) for $Pr_m \geqslant 1$. Closer inspection of $Pr_m \leqslant 1$ data in the range in figures 13(a) and 14(a) show no apparent trend as Pr_m decreases. This is in contrast to the distinct downward slope found in the data from the decaying simulations.

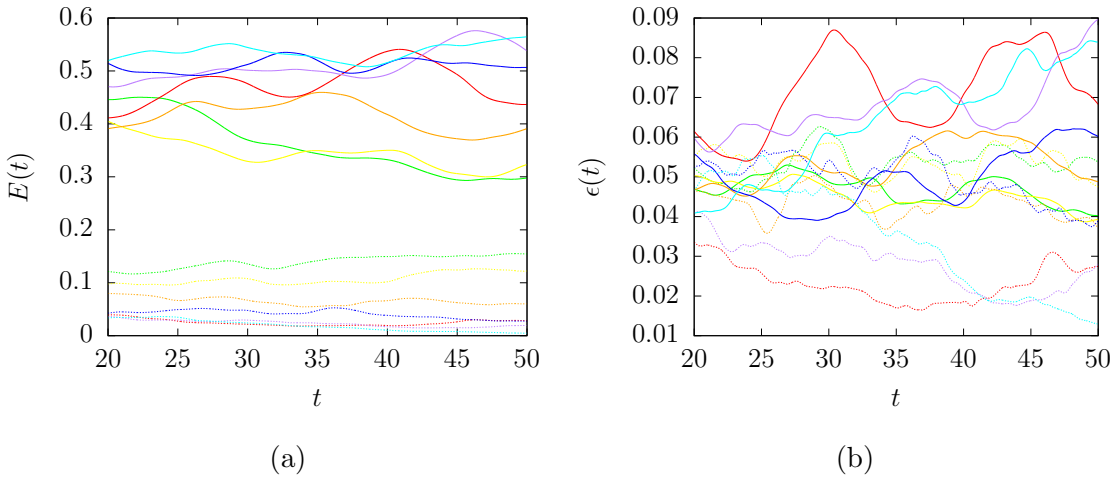

Figure 13. Magnetic/kinetic energy (a), and magnetic/kinetic dissipation (b), where kinetic values are represented by solid lines and magnetic values by dashed lines. The key used is the same as in figures 9 and 10.

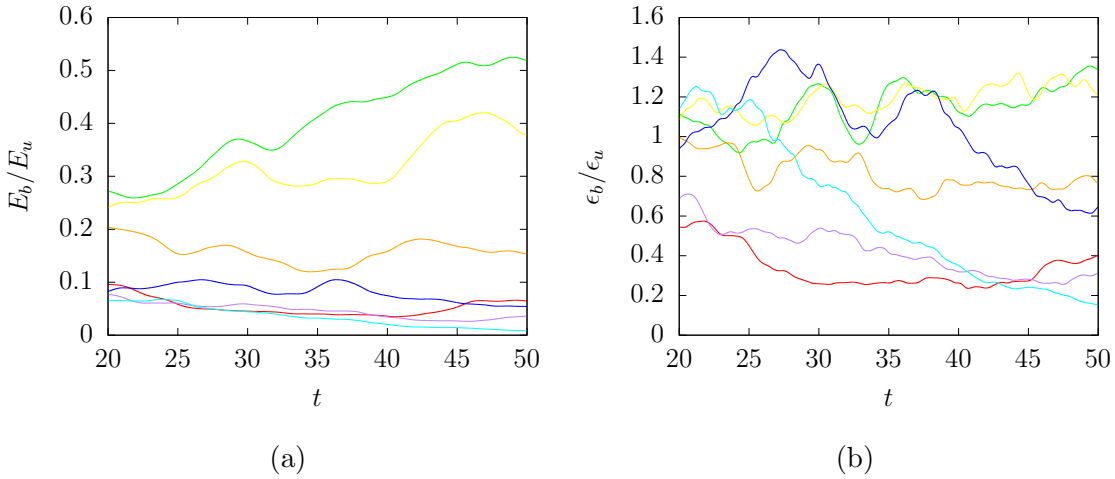

Figure 14. Ratio of magnetic to kinetic energy (a), and magnetic to kinetic dissipation (b). The key used is the same as in figures 9 and 10.

Figure 13(b) shows the magnetic and kinetic dissipation over time, and figure 14(b) shows the evolution of the ratio of these quantities over time. The behaviour seen here is quite erratic, and the clear pattern we had hoped to find by varying the Prandtl number is absent. The effects of this in the time averaged case are discussed in section 5.3.1.

For comparison, results from Sahoo et al. have been included (figure 15), where a clear difference between the kinetic and magnetic dissipation can be seen. As the magnetic Prandtl number is increased, the spacing between the magnetic and kinetic dissipation decreases, which might help to explain some of the disparities in the time averaged results discussed in the following section.

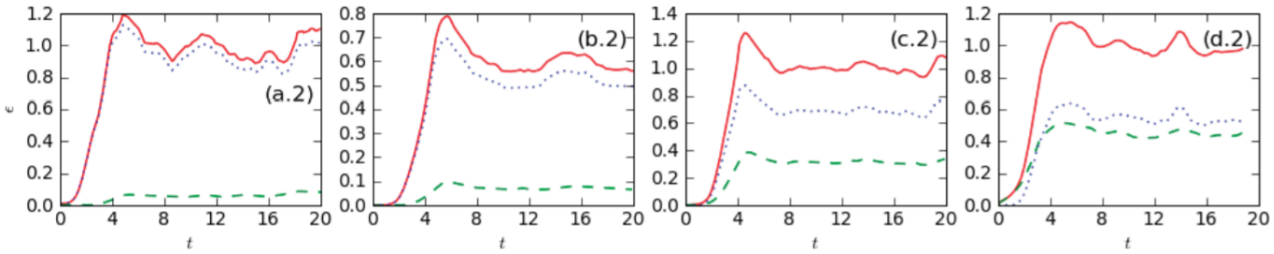

Figure 15. Plots of dissipation over time from Sahoo et al., 2011[4]. Total dissipation, $\epsilon_u + \epsilon_b$ is represented by the red line, kinetic dissipation is represented by the dashed green line and magnetic dissipation by the dashed blue line. Data for $Pr_m = 0.01$ is shown plot (a.2), $Pr_m = 0.1$ in plot (b.2), $Pr_m = 1$ in plot (c.2), and $Pr_m = 10$ in plot (d.2). Note that different units have been used to measure time, so cannot compare directly to data in 13(b)

5.3 Further Results and Discussion

5.3.1 Energy Ratio

In the work of Haugen et al., 2003[17] some scaling of $\frac{E_b}{E_u}$ with the magnetic Reynolds number was suggested, for simulations with $Pr_m = 1$, where different values of Re_m were obtained by varying η and ν together. Results for $\frac{E_b}{E_u}$ in sections 5.1 and 5.2, agree with this hypothesis, and are shown to increase with Re_m (figures 16 and 17) with a slope of 5×10^{-3} for decaying simulations and 5×10^{-4} for stationary simulations. However, this is only valid in the region $Pr_m \geqslant 1$, as there is little variation in Re_m below this value, due to the decision to vary ν rather than η to obtain data for $Pr_m < 1$.

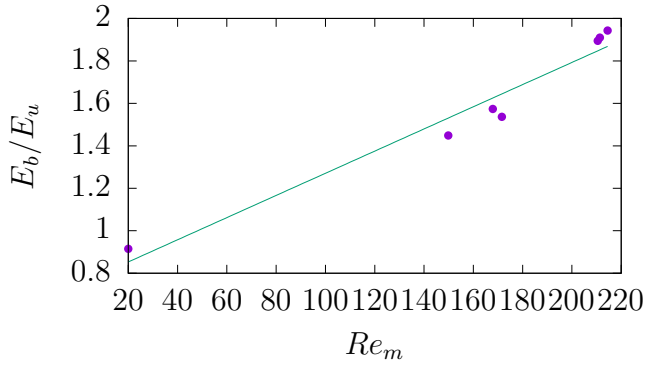

Figure 16. Graph of energy ratio vs. Re_m for decaying simulations.

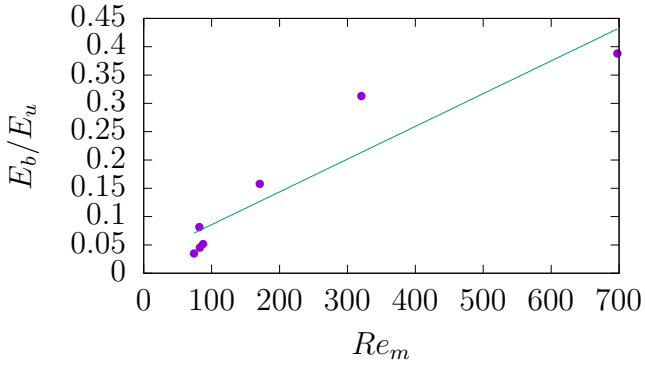

Figure 17. Graph of energy ratio vs. Re_m for stationary simulations.

Further simulations would need to be run with more varying η for $Pr_m < 1$. This would require larger lattice sizes, as the simulation would cease to exhibit any turbulent behaviour if ν was increased any further. Running hese additional simulations would help to confirm if the difference in slope in the two graphs is a product of the different values of ν and η used in each case, or whether the simulation was stationary or decaying impacts this result.

5.3.2 Dissipation Ratio

Sahoo et al. [4] found that the difference between kinetic and magnetic dissipation decreases as we increase the Prandtl number from about 1 at $Pr_m = 0.01$ to close to 0 at $Pr_m = 10$ for forced and decaying simulations. They also found that the ratio between kinetic and magnetic energy increases as we increase the Prandtl number from about 0.2 at $Pr_m = 0.01$ to approximately 1 at $Pr_m = 10$.

Brandenburg et al. have examined the dissipation ratio in [5, 8] and found strong agreement with results in [4] that the dissipation ration scaled with Pr_m as a power law:

$$\frac{\epsilon_u}{\epsilon_b} \propto Pr_m^q. \tag{5.4}$$

For decaying turbulence results from Sahoo et al.[4] were analysed by Brandenburg et al.[5] and this relationship was found to be $\frac{\epsilon_u}{\epsilon_b} = 0.6Pr_m^{0.55}$. Measurements taken at the peak of dissipation from the high resolution decaying simulations in this project show good agreement with these results, and a relationship of $\frac{\epsilon_u}{\epsilon_b} = 0.7Pr_m^{0.58}$ was found. As the decaying data has only 3 distinct values of Pr_m, more simulations would need to be run at intermediary Prandtl numbers to determine the accuracy of this result.

For non-helical forced turbulence Brandenburg et al. found the value of q to be 0.95 for $Pr_m \leqslant 1$ and 0.55 for $Pr_m \geqslant 1$, and for helical forcing, q was found to be 0.6[8, 5] for all values of Pr_m.

However, time averaged results from our stationary simulations show no correlation with this, and appear totally random (figure 18), despite using a similar forcing method as Sahoo et al.[4]. The remainder of this section will focus on possible reasons for this.

Data close to $Pr_m = 1$ is all very well resolved and yet shows no agreement To completely rule out the possibility of this being an error due to inaccuracies caused by resolution, data for $Pr_m \geqslant 1$ in this report was compared to other non helical forced data[4] obtained from the same code with the same viscosity but a higher resolution. There was strong agreement between results, ruling out the possibility of resolution issues.

The main difference between simulations run here and simulations in Sahoo et al.[4] and Brandenburg et al.[5] were the values of viscosity used. Running simulations at a lower viscosity would require a much bigger box size, and in turn a lot more time to run. In

[4]these simulations were run by Mairi McKay and have been referenced with permission

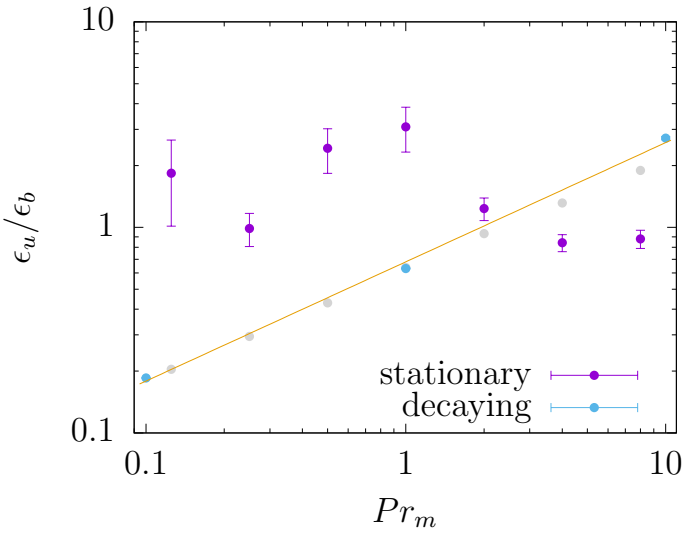

Figure 18. Graph of dissipation ratio vs Pr_m for stationary and decaying simulations. Errors are included on time averaged values.

addition to this, as the lattice size is increased the timestep must be decreased and the forcing rate rescaled accordingly. Therefore there was not time to run further high resolution forced simulations at lower viscosities within the time frame of this project. Further study could be done in this area to examine if results in [4, 8, 5] are viscosity dependent.

It is also possible that the erratic behaviour discussed in figures 13 and 14, is a result of the forcing function. This is unlikely, as the same forcing function has been used in Sahoo et al.[4]. However, before the forced runs reach a steady state, the behaviour of the spectra at this point in time is closer to that of the decaying simulations. The points marked in grey in figure 18 are taken from the peak of dissipation of the stationary simulations, and closely follow the line observed in the decaying data. This suggests the anomaly is due to either the forcing function or its implementation, or, more likely, a viscosity related effect that only comes in to play only in the steady state.

6 Conclusion

Across all the simulations performed, results for the energy and dissipation spectra mostly agreed with results for varying Prandtl number found in Sahoo et al.[4] and Brandenburg et al.[5].

In agreement with results in Haugen et al.[17], a linear dependence between the ratio of magnetic to kinetic energy and magnetic Prandtl number was found. More simulations with varying values for the resistivity would need to be run to confirm the accuracy of this.

Examining the dissipation ratio, a relationship of $\frac{\epsilon_u}{\epsilon_b} = 0.6 Pr_m^{0.55}$ was found for the decaying simulations. No power law dependence could be found from the results of the stationary

simulations. This is most likely an effect of the relatively low kinetic Reynolds numbers used, and would be an interesting area of further study. With the rapid advancement of processing power, high resolution runs with larger lattice sizes could be run for the same range of Pr_m. Varying η and ν together at each value of Pr_m could determine if a critical value of η or ν must be reached before the power result found by Brandenburg et al.[5] can be seen.

Acknowledgements

I would like to thank Prof. Arjun Berera for his help and support throughout this project. I would also like to extend my gratitude to Mairi MacKay for her constant guidance and support, as well as for providing me with her data. I would like to thank Richard Ho, as well as Mairi, for answering any questions I had and teaching me the intricacies of using the code.

References

[1] W. D. McComb. *The Physics of Fluid Turbulence*. Clarendon Press, 1992.

[2] D. Biskamp. *Magnetohydrodynamic Turbulence*. Cambridge University Press, 2008.

[3] S. R. Yoffe. *Investigation of the transfer and dissipation of energy in isotropic turbulence*. PhD thesis, University of Edinburgh, 2012.

[4] G. Sahoo, P. Perlekar, and R. Pandit. Systematics of the magnetic-prandtl-number dependence of homogeneous, isotropic magnetohydrodynamic turbulence. *New Journal of Physics*, 13(1):013036, 2011.

[5] A. Brandenburg. Magnetic prandtl number dependence of the kinetic-to-magnetic dissipation ratio. *The Astrophysical Journal*, 791(1):12, 2014.

[6] D. F. Harlacher, H. Klimach, and S. Roller. Turbulence simulation at large scale. *inSiDe*, 10, 2012.

[7] M. K. Verma. Statistical theory of magnetohydrodynamic turbulence: recent results. *Physics Reports*, 401(56):229 – 380, 2004.

[8] A. Brandenburg. Nonlinear small-scale dynamos at low magnetic prandtl numbers. *The Astrophysical Journal*, 741(2):92, 2011.

[9] N. Popovie. Applied dynamical systems (math 11140). University Lecture Notes, 2016.

[10] J.C.R. Hunt, O.M. Phillips, and D. Williams. *Turbulence and Stochastic Processes: Kolmogorov's Ideas 50 Years on*. Philosophical Transactions of the Royal Society, Series B. Royal Society, 1991.

[11] H. K. Moffatt. *Reflections on Magnetohydrodynamics*. Cambridge University Press, 2000.

[12] H. K. Moffatt. The degree of knottedness of tangled vortex lines. *Journal of Fluid Mechanics*, 35(1):117129, 1969.

[13] U. Frisch, A. Pouquet, J. LOrat, and A. Mazure. Possibility of an inverse cascade of magnetic helicity in magnetohydrodynamic turbulence. *Journal of Fluid Mechanics*, 68(4):769778, 1975.

[14] M. F. Linkmann. *Self-organisation processes in (magneto)hydrodynamic turbulence*. PhD thesis, University of Edinburgh, 2016.

[15] A. A. Schekochihin, Steven C. Cowley, Samuel F. Taylor, Jason L. Maron, and James C. McWilliams. Simulations of the small-scale turbulent dynamo. *The Astrophysical Journal*, 612(1):276, 2004.

[16] A. Brandenburg, D. Sokoloff, and K. Subramanian. Current Status of Turbulent Dynamo Theory. From Large-Scale to Small-Scale Dynamos. *Space Science Reviews*, 169:123–157, September 2012.

[17] N. E. L. Haugen, A. Brandenburg, and W. Dobler. Is Nonhelical Hydromagnetic Turbulence Peaked at Small Scales? *The Astrophysical Journal*, 597:L141–L144, November 2003.

[18] D. Gonze. Numerical methods for ordinary differential equations. University Lecture Notes.

[19] W.C. Muller and D. Biskamp. Scaling properties of three-dimensional magnetohydrodynamic turbulence. *Phys. Rev. Lett.*, 84:475–478, January 2000.

[20] J. A. Merrifield, S. C. Chapman, and R. O. Dendy. Intermittency, dissipation, and scaling in two-dimensional magnetohydrodynamic turbulence. *Physics of Plasmas*, 14(1):012301, 2007.

Appendices

A Glossary of Important Terms

ν ..... kinematic viscosity

η ..... magnetic resistivity

$Re = \frac{UL}{\nu}$ ..... kinetic Reynolds number

$Re_m = \frac{UL}{\eta}$ ..... magnetic Reynolds number

$Pr_m = \frac{\nu}{\eta}$ ..... magnetic Prandtl number

$E_u(t)$ ..... total kinetic energy at time t

$E_b(t)$ ..... total magnetic energy at time t

$E_u(k)$ ..... stationary kinetic energy spectrum

$E_b(k)$ ..... stationary magnetic energy spectrum

$\epsilon_u(t)$ ..... rate of kinetic dissipation at time t

$\epsilon_b(t)$ ..... rate of magnetic dissipation at time t

$\epsilon_u(k)$ ..... stationary kinetic dissipation spectrum

$\epsilon_b(k)$ ..... stationary magnetic dissipation spectrum

$l_D^u = \left(\frac{\nu^3}{\epsilon_u}\right)^{\frac{1}{4}}$ ..... Kolmogorov microscale

$l_D^b = \left(\frac{\eta^3}{\epsilon_b}\right)^{\frac{1}{4}}$ ..... magnetic dissipative microscale

$k_D^u = \left(\frac{\epsilon_b}{\nu^3}\right)^{\frac{1}{4}}$ ..... Kolmogorov wavenumber

$k_D^b = \left(\frac{\epsilon_b}{\eta^3}\right)^{\frac{1}{4}}$ ..... magnetic dissipative wavenumber